Journal of Materials Chemistry A

Accepted Manuscript

ROYAL SOCIETY OF CHEMISTRY

www.rsc.org/materialsA

Journal of Materials Chemistry A

ARTICLE

Simultaneous enhancement in power factor and thermoelectric performance of copper sulfide by In_2S_3 doping

Received 00th January 20xx,
Accepted 00th January 20xx

DOI: 10.1039/x0xx00000x

www.rsc.org/

Qing-Long Meng,[a,‡] Shuang Kong,[a,b‡] Zhiwei Huang,[a,b] Yuanhu Zhu,[a] Heng-Chang Liu,[a,c] Xiaowei Lu,[a,b] Peng Jiang[a,*] and Xinhe Bao[a]

In this work, we demonstrate simultaneously enhanced power factor and thermoelectric performance in Cu_2S upon the introduction of In_2S_3. The evident improvement in electrical conductivity, coupling with less affected Seebeck coefficient, leads to a high power factor of 1361 μW m^{-1} K^{-2} at 850 K, which is much higher than those previously reported values for Cu_2S-based thermoelectric materials. Along with moderate thermal conductivity, a high *ZT* value of 1.23 at 850 K is achieved. Interestingly, the phase transitions and copper segregation of Cu_2S are also suppressed by In_2S_3 doping due to the formation of nanoscale $CuInS_2$ phase. Such a high power factor, together with a decent *ZT* value and suppressed phase transition and copper segregation, will be beneficial to its practical applications in thermoelectric power generation.

1. Introduction

More than 60% of the world's consumed energy is lost as waste heat,[1] and therefore great efforts have been made to develop technologies harvesting the waste heat efficiently. As one of the promising waste heat harvesting technologies, thermoelectric materials and devices have attracted considerable interest in recent decades because they offer a promising route to convert waste heat into electrical power. The efficiency of thermoelectric materials is theoretically quantified by the dimensionless figure of merit (*ZT*), which is defined as $ZT=(S^2\sigma/\kappa)T$, where *S*, σ, κ and *T* are the Seebeck coefficient, electrical conductivity, thermal conductivity and absolute temperature of themoelectric materials, respectively.

Usually, there are two alternative strategies to achieve high performance (*ZT*): either by κ reduction or by power factor ($PF=S^2\sigma$) enhancement. In recent years, significant achievements have been accomplished to improve *ZT* by κ reduction, such as "rattling" scattering,[2, 3] grain-boundary scattering,[4, 5] panoscopic scattering (all length-scale phonon scattering),[6-8] anharmonic phonon scattering,[9, 10] interface scattering in thin films and nanowires.[11-13] These efforts have successfully reduced κ to approach the amorphous limit. There are also several effective approaches to enhance the power factor, like resonant doping,[14] carrier energy filtering,[15, 16] and band convergence.[17]

Searching for novel materials with excellent performance and without using heavy and toxic elements is the goal for thermoelectric research and practical applications. Among various materials, copper sulfide ($Cu_{2-x}S$) is a promising candidate and has received great attention because it is composed of non-toxic and earth-abundant elements, and beneficial for its large-scale practical applications. Additionally, it exhibits high thermoelectric performance due to its exceptionally low thermal conductivity and decent power factor in the moderate and high temperature range.[18-20] Recently, it has been reported that Cu_2S with slightly copper deficiency exhibits excellent thermoelectric performance with high *ZT* values ~ 1.7 at 1000 K.[19] Zhao et al. further enhanced *ZT* as high as 1.9 at 973 K using a melt-solidification technique.[18] It is worth noting that *ZT* is not the only concern for practical applications. The output power density is equally as important as *ZT* or more important for power generation when the heat source is unlimited or free.[21, 22] The output power density is quantified as $\omega=(T_h-T_c)^2PF/4L$, where T_h, T_c, and *L* are the hot side temperature, cold side temperature, and thermoelectric leg length, respectively.[21, 22] Therefore, it is of great importance to enhance thermoelectric performance for copper sulfide by improving power factor from the viewpoint of power generation.[21, 22] Additionally, the issues regarding segregation of metallic copper and phase transitions of copper sulfide are also primary concerns for practical applications.[23, 24]

Herein, we report that the simultaneous enhancement in power factor and thermoelectric performance of Cu_2S can be achieved by a simple In_2S_3 doping approach. The power factor of Cu_2S is enhanced significantly up to 1361 μW m^{-1} K^{-2} at about 850 K, which is more than 13 times higher than that of undoped Cu_2S and

[a] State Key Laboratory of Catalysis, Dalian Institute of Chemical Physics, Chinese Academy of Sciences, Dalian 116023, China. *Email: pengjiang@dicp.ac.cn xhbao@dicp.ac.cn
[b] University of Chinese Academy of Sciences, Beijing 100039, China
[c] School of Physical Science and Technology, ShanghaiTech University, Shanghai 200031, China.
‡ These authors contribute equally.
† Footnotes relating to the title and/or authors should appear here.
Electronic Supplementary Information (ESI) available: [details of any supplementary information available should be included here]. See DOI: 10.1039/x0xx00000x

even higher than those previously reported values for Cu_2S-based thermoelectric materials with high *ZT*.[18-20] This effective enhancement of power factor is attributed to the greatly improved electrical conductivity along with decent Seebeck coefficient. Due to the improvement of power factor, a *ZT* value of 1.23 is achieved at 850 K. Additionally, the phase transitions and copper segregation are also suppressed by In_2S_3 doping. Thus, the simultaneous enhancement in power factor and thermoelectric performance, together with suppressed phase transition and copper segregation, promises its practical applications in thermoelectric power generation.

2. Experimental

2.1 Sample preparation

Reagent chemicals were used as obtained: Cu_2S (Alfa-Aesar, 99.5%) and In_2S_3 (Alfa-Aesar, 99.98%). Cu_2S and In_2S_3 were weighted according to the specified molar ratios of Cu_2S-xIn_2S_3 (x=0, 1%, 2%, 5% and 10%), and then the weighted chemicals were fully mixed and ground with agate mortar and pestle for 30 minutes. The mixed fine powders were then densified by spark plasma sintering system (LABOX-650, SINTER LAND) at 873 K under uniaxial pressure of 50 MPa for 5 minutes in a 12.7 mm diameter graphite die.

2.2 Sample characterization

X-ray diffraction (XRD) patterns were performed by a PANalytical EMPYREAN system with Cu K_α radiation (λ=1.542 Å). The measurement was conducted at a 2 theta range of 20^o – 50^o at room temperature with a scanning rate of 13.5 degree/min. Hall measurements were performed with a commercial instrument (HL5500PC). The squared sample with a thickness less than 500 μm was placed in a vacuum with an applied magnetic field (0.51 T) perpendicular to its surface. The resistivity (ρ) and Hall coefficient (R_H) were measured by the van de Pauw method. The Hall carrier mobility (μ) was calculated by $\mu=R_H/\rho$, and the Hall carrier concentration n_H by $n_H=1/(eR_H)$. Scanning electron microscopy (SEM) characterization was performed on an FEI QUANTA 200 FEG microscope at 20 KV. Transmission electron microscopy (TEM) characterization was carried out on a JEM-2100 microscope.

2.3 Performance measurement

The electrical transport properties (Seebeck coefficient and electrical conductivity) of Cu_2S-xIn_2S_3 (x=0, 1%, 2%, 5% and 10%) were measured simultaneously using an ULVAC-RIKO ZEM 3 system under low-pressure helium gas. The experiments were repeated twice for each sample. The measurement of thermal diffusivity was performed by the lasher flash method (Netzsch, LFA 457, Germany). Before the measurement, the sample was coated with a thin layer of graphite by graphite spray (Graphite33) to avoid errors from the emissivity from the sample. The specific heat capacity was calculated from the differential scanning calorimetric results (Netzsch, STA 449, Germany). The density was measured by the Archimedes method. The thermal conductivity was calculated via the equation $\kappa=\rho DCp$ (κ is the thermal conductivity, ρ is the density, D is the thermal diffusivity, Cp is the specific heat capacity).

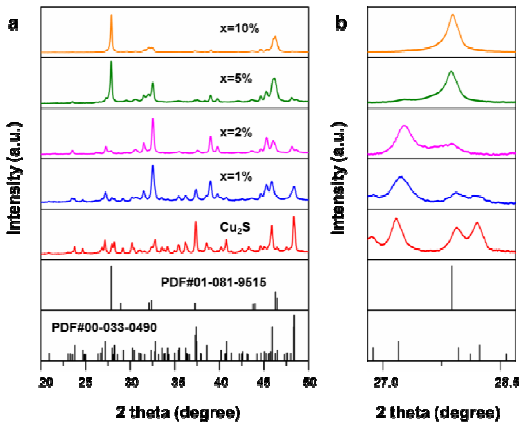

Fig. 1 Powder XRD patterns of Cu_2S-xIn_2S_3 (x=0, 1%, 2%, 5% and 10%). **a.** Powder XRD patterns. **b.** Enlarged powder XRD patterns.

3. Results and Discussion

3.1 Sample characterization

Powder x-ray diffraction (XRD) patterns of undoped and doped Cu_2S with different nominal compositions are given in **Fig. 1**. The x-ray diffraction patterns of the undoped Cu_2S are well indexed as monoclinic Cu_2S (JCPDS No. #00-033-0490). After In_2S_3 doping, the monoclinic Cu_2S phase diminishes gradually and the tetragonal $CuInS_2$ phase (JCPDS No. #01-081-9515) becomes detectable, especially for heavily doped Cu_2S as shown in **Fig. 1b**. Therefore, it can be believed that the doped samples are a two-phase composite, composed of undoped monoclinic Cu_2S phase and doped tetragonal $CuInS_2$ phase.

The microstructure features of undoped and doped Cu_2S have been investigated by SEM, shown in **Fig. 2** and **Fig. S1**. After doping In_2S_3, the morphology of Cu_2S changes apparently and the grain boundaries decrease significantly. Energy dispersive X-ray spectrometer (EDX) elemental mapping results demonstrate that, for doped Cu_2S samples, the Cu, In and S elements are not uniformly distributed at the microstructural level (**Fig. S2 – Fig. S5**). As shown in the TEM image of Cu_2S-2%In_2S_3 (**Fig. 3**), some nanoparticles, ranging from several nanometers to 100 nm, can be clearly observed in the Cu_2S matrix. The composition of these nanoparticles can be further identified to $CuInS_2$ phase by EDX analysis (**Fig. 3** and **Fig. S6**). This result is also confirmed by HR-TEM, and the lattice spacing of 3.2 Å corresponds to the (112) planes of $CuInS_2$ (**Fig. 3** Inset), consistent with the XRD results (**Fig. 1**).

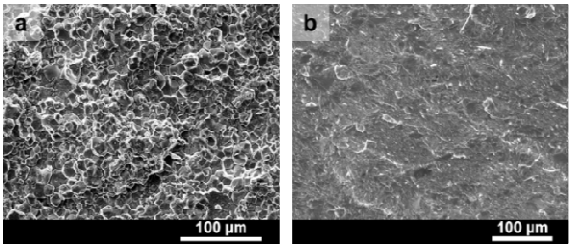

Fig. 2 SEM images of Cu_2S and Cu_2S-2%In_2S_3. **a.** Cu_2S. **b.** Cu_2S-2%In_2S_3.

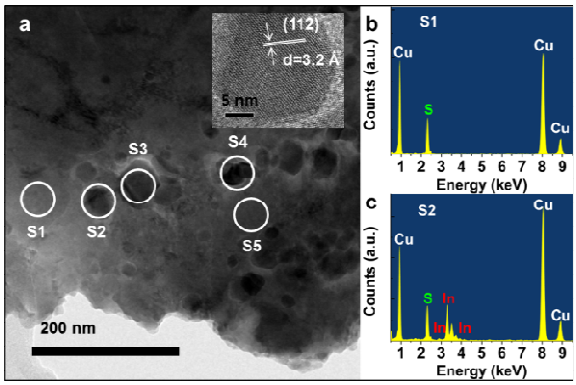

Fig. 3 TEM image and EDX spectra of Cu_2S-2%In_2S_3. **a.** TEM image. **b.** EDX spectrum of Spot1 (S1). **c.** EDX spectrum of Spot2 (S2). The inset shows HR-TEM image.

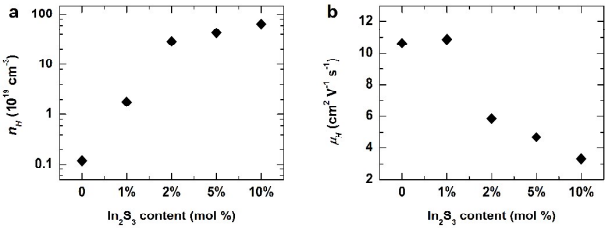

Fig. 4 Hall carrier concentration and mobility as a function of doped In_2S_3 content at 325 K. **a.** Hall carrier concentration. **b.** Hall carrier mobility.

Hall measurements were carried out at 325 K to estimate the carrier concentration and carrier mobility for undoped and doped Cu_2S (**Fig. 4**). The carrier concentration at 325 K is 1.18×10^{18} cm^{-3} for Cu_2S, and then increases to 2.91×10^{20} cm^{-3} for Cu_2S-2%In_2S_3, and further reaches 6.47×10^{20} cm^{-3} for Cu_2S-10%In_2S_3. Notably, upon In_2S_3 doping, the carrier concentration is improved more than two orders of magnitude, while the carrier mobility is less affected. Based on Eq. (1) and Eq. (2), we can conclude that these two parameters could contribute to a considerable increase in electrical conductivity, and decrease in Seebeck coefficient.[25]

$$\sigma = ne\mu \qquad \text{Eq. (1)}$$

$$S = \frac{8\pi^2 k_B^2}{3eh^2} m^* T \left(\frac{\pi}{3n}\right)^{2/3} \qquad \text{Eq. (2)}$$

where σ, n, μ, S and m^* are the electrical conductivity, carrier concentration, carrier mobility, Seebeck coefficient and effective mass of the carrier, respectively.[25]

3.2 Simultaneous enhancement in *ZT* and power factor enhancement by In_2S_3 doping

Combining the electrical and thermal transport properties, the calculated *ZT* values of undoped and doped Cu_2S are shown in **Fig. 5a**. Upon In_2S_3 doping, *ZT* is enhanced considerably. The

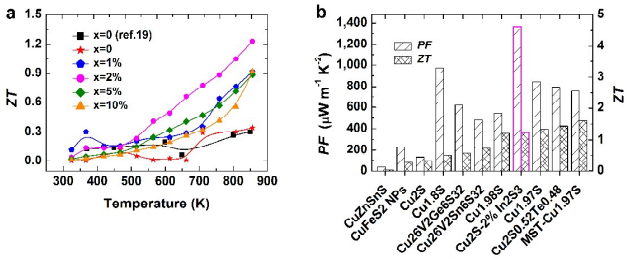

Fig. 5 a. Temperature-dependent *ZT* values of Cu_2S-xIn_2S_3 (x=0, 1%, 2%, 5% and 10%). **b.** Comparison of *ZT* and power factors of Cu_2S-based materials in this work and previous reports. (CuZnSnS,[26] $CuFeS_2$ NPs,[27] Cu_2S,[19] $Cu_{1.8}S$,[20] $Cu_{26}V_2Ge_6S_{32}$,[28] $Cu_{26}V_2Ge_6S_{32}$,[28] $Cu_{1.98}S$,[19] $Cu_{1.97}S$,[19] $Cu_2S0.52Te_{0.48}$,[29] MST-$Cu_{1.97}S$.[18] Here, the columns with magenta border lines in **Fig. 5b** stand for the power factor and *ZT* of Cu_2S-2%In_2S_3 in this work.

maximum *ZT* value of 1.23 at 850 K is achieved for the Cu_2S-2%In_2S_3, which is more than 3.5 times higher than that of undoped Cu_2S (*ZT*=0.34). More importantly, the power factor of 1361 μW m^{-1} K^{-2} at 850 K is achieved for the Cu_2S-2%In_2S_3, which is more than 13 times higher than undoped Cu_2S. **Fig. 5b** compares the power factor and *ZT* of Cu_2S-2%In_2S_3 in this work with those of Cu_2S-based materials in previous reports. The Cu_2S-2%In_2S_3 exhibits much higher power factor than other Cu_2S-based materials reported in previous work.[18-20, 26-29] Moreover, Cu_2S-2%In_2S_3 also shows comparable *ZT* with the highest reported *ZT* values for Cu_2S-based materials.[18, 19, 29]

3.3 Electrical transport properties

Figure 6a shows the temperature-dependent electrical conductivities of undoped and doped Cu_2S. The electrical conductivity of Cu_2S exhibits a dramatic enhancement upon In_2S_3 doping. For example, the electrical conductivity of Cu_2S-2%In_2S_3 is improved more than 4 orders of magnitude at room temperature compared with undoped Cu_2S. This evident increase in electrical conductivity is attributed to the pronounced increase in Hall carrier concentrations. The electrical conductivities of doped Cu_2S (Cu_2S-xIn_2S_3, x=2%, 5% and 10%) first increase at low temperatures, and then decrease with increasing temperature, exhibiting the behavior typical of semiconductors at low temperatures and metals at high temperatures. Such a temperature dependent behavior of electrical conductivity for doped Cu_2S is totally different from that of pristine Cu_2S,[19] which might be intimately related to the suppression of phase transition with increasing temperature, as evidenced by the temperature-dependent specific heat capacity (**Fig. 8**). The doped Cu_2S (Cu_2S-xIn_2S_3, x=2%, 5% and 10%) shows peak values in electrical conductivity in the temperature range of 510 – 570 K. Notably, the electrical conductivity of Cu_2S-2%In_2S_3 reaches the maximum value of 8.54×10^4 S m^{-1} at about 570 K, which is much higher than previously reported value by introducing copper deficiency in Cu_2S ($Cu_{1.97}S$, about 1.00×10^4 S m^{-1}).[19]

The temperature-dependent Seebeck coefficients of undoped and doped Cu_2S, as shown in **Fig. 6b**, reveal that the Seebeck coefficients are positive, suggesting a p-type electrical transport behavior with holes as charge carriers, which might be caused by its intrinsic properties of copper deficiency.[29] The Seebeck coefficient

Journal of Materials Chemistry A

ARTICLE

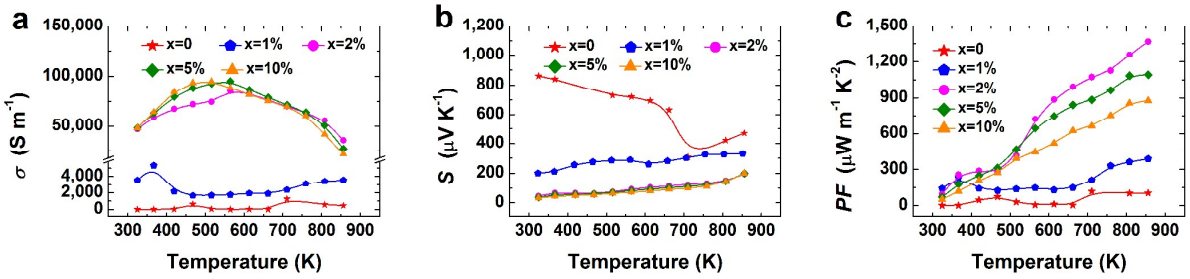

Fig. 6 Temperature-dependent electrical transport properties of Cu_2S-xIn_2S_3 (x=0, 1%, 2%, 5% and 10%). **a.** Electrical conductivity. **b.** Seebeck coefficient. **c.** Power factor.

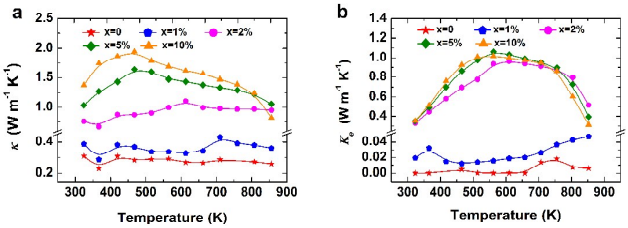

Fig. 7. Temperature-dependent thermal conductivity of Cu_2S-xIn_2S_3 (x=0, 1%, 2%, 5% and 10%). **a.** Total thermal conductivity. **b.** Electronic thermal conductivity.

of Cu_2S decreases in the temperature range of 325 – 700 K, then increase above 700 K. Notably, the Seebeck coefficients drop drastically in the temperature range of 650 – 700 K. Such a temperature dependent behavior of Cu_2S is expected to be related to the phase transition,[19] which is also evidenced by the temperature dependence of specific heat capacity (**Fig. 8**). With increasing In_2S_3 doping content, the Seebeck coefficient values decrease significantly, which is consistent with the increase in carrier concentrations. The Seebeck coefficients of doped Cu_2S increase monotonically with temperature in the investigated temperature range. Unlike undoped Cu_2S, the suddenly dramatic decrease in the Seebeck coefficients in the temperature range of 650 – 700 K disappears gradually with In_2S_3 doping (**Fig. 6b**), which is due to the phase transition suppression.

The power factor is enhanced significantly by In_2S_3 doping (**Fig. 6c**), especially for 2 mol% In_2S_3 doping, which is improved more than 13 times compared with undoped Cu_2S. Such an evident enhancement in the power factor is attributed to the strongly enhanced electrical conductivity and less affected Seebeck coefficient. Among doped samples, Cu_2S-2%In_2S_3 exhibits strikingly high power factor value of 1361 μW m^{-1} K^{-2} at 850 K, which is higher than those previously reported values for Cu_2S-based thermoelectric materials by different groups.[18-20, 26-29] Such a high power factor value is comparable with the state-of-the-art hole-doped single-crystal SnSe.[1] Therefore, such a high power factor value is definitely beneficial for practical applications from the view point of power generation.[21, 22]

3.4 Thermal transport properties

Figure 7 compares the temperature-dependent thermal conductivities of undoped and doped Cu_2S. The undoped Cu_2S exhibits ultralow intrinsic thermal conductivity, which is comparable to previously reported values.[18, 19] The total thermal conductivity (κ_{tot}) shows an increasing trend with increasing In_2S_3 doping content. According to Wiedemann–Franz relation, the electronic thermal conductivity (**Fig. 7b**) can be calculated by the equation of $\kappa_e=L\sigma T$ (where L is the Lorenz number, which was determined based on the Seebeck coefficient measurements ($L=1.5+exp[-|s|/116]$), as proposed by Kim and Snyder et al[30]). The contribution of electronic thermal conductivity to total thermal conductivity increases significantly due to a dramatic increase in electrical conductivity after In_2S_3 doping. Therefore, the rise in the total thermal conductivity after In_2S_3 doping is attributed to the significant increase in the electronic thermal conductivity (κ_e).

3.5 Suppression of phase transition and copper segregation

Upon In_2S_3 doping, the temperature-dependent specific heat capacity of Cu_2S changes significantly and the phase transitions of Cu_2S at about 400 K and 700 – 740 K are evidently suppressed (**Fig. 8**). The suppression of phase transition is consistent with the suppression of copper segregation (**Fig. S7**), which can be easily observed at the surface of the pressed Cu_2S columns after the synthesis process by SPS.

The phase transition and copper segregation of Cu_2S are related to the facile Cu-ion migration, which can be characterized by the change of relative electrical resistance (R/R_0, R_0 and R are the initial electrical resistance and the electrical resistance, respectively)[24, 31] in the current stress test as proposed by Chen's

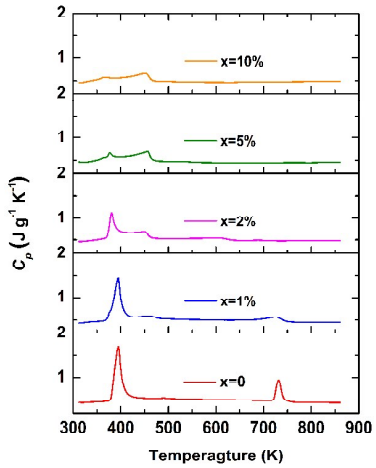

Fig. 8 Temperature-dependent specific heat capacity of Cu_2S-xIn_2S_3 (x=0, 1%, 2%, 5% and 10%).

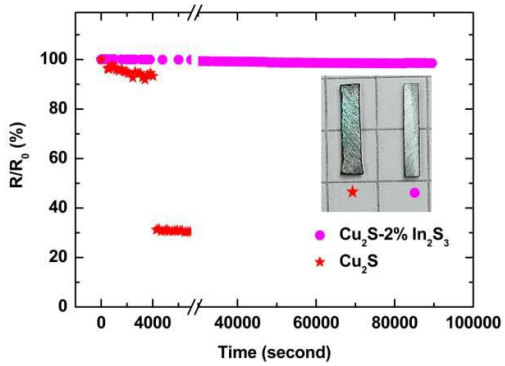

Fig. 9 Time-dependent relative electrical resistance of Cu_2S and Cu_2S-2%In_2S_3 under a large current density (12 A cm^{-2}) at 573 K. The inset shows the images of Cu_2S (left) and Cu_2S-2%In_2S_3 (right) after the current stress test.

group because Cu-ion migration leads to a decrease in electrical resistance.[19, 31] Herein, we use the maximum standard current density (12 A cm^{-2}) in thermoelectric property measurement system (ZEM 3) to evaluate the Cu-ion migration at 573 K, and these conditions are the same to the previous reports.[24, 31] As shown in Fig. 9, the R/R_0 of Cu_2S drops abruptly to about 30% after 4000 s. Such a significant variation of R/R_0 may be caused by the significant copper segregation.[31, 32] In the case of Cu_2S-2%In_2S_3, there is no obvious decrease in R/R_0 even after 90000 s. Furthermore, the sample of Cu_2S shows an obvious copper segregation and distortion after current stress test (**Fig. 9** Inset). After In_2S_3 doping, the sample shows no obvious difference before and after current stress test. Therefore, the less variation of R/R_0 and sample status after the current stress test suggests that Cu_2S becomes more stable after In_2S_3 doping. This stability enhancement is consistent with the phase suppression by In2S3 doping, as evidenced in the temperature-dependent C_p results (Fig. 8).

It is widely acknowledged that doping can suppress the phase transition.[33-40] The well-known anatase-to-rutile phase transition can be significantly inhibited by doping either metals,[35, 36] metalloids[37] or metal oxides[38-40] due to the reduction in oxygen vacancies or formation of interstitial atoms, which prevent the nucleating process for anatase-to-rutile phase transition (Ti and O atoms rearrangement). In addition, the thermoelectric material Zn_4Sb_3 shows evident β to α/α' phase transition, which can be fully inhibited by In or Ag doping,[33, 34] because the replacement of dopant atoms for interstitial Zn atoms can impede the motion and diffusion of Zn atoms (ions). Therefore, after doping, the substitution of original atom sites in the host lattice by foreign atoms triggers the compositional and structural changes in the host matrix, which suppress the phase transition of the host matrix by impeding the motion or diffusion of the host atoms.

For Cu_2S, the phase transition occurs once the positions of the Cu atom move from ordered states to disordered states by Cu-ion migration or diffusion.[20, 41] After Cu_2S doped by In_2S_3, the Cu ions incorporate into the In_2S_3 lattice to form nanoscale $CuInS_2$ particles with chalcopyrite structure[42, 43] as suggested by XRD and HR-TEM (**Fig. 1** and **Fig. 3**). These nanoscale $CuInS_2$ particles can possibly serve as "obstacles" to block the Cu-ion migration channels to suppress phase transition by impeding the Cu-ion migration or diffusion, as confirmed by the current stress test (**Fig. 9**). This is similar to the case of the pinning effect in Cu_5FeS_4 reported by Chen's group, in which the atomic-scale Fe ions serve as blockers for Cu-ion migration. Thus, In_2S_3 doping can suppress the phase transition and copper segregation of Cu_2S, which is greatly beneficial for practical applications.

4. Conclusions

In summary, In_2S_3 doping has been shown to be a facile and effective route to simultaneously enhance the power factor and thermoelectric performance of Cu_2S. The dramatic increase in carrier concentrations leads to the highly enhanced power factor and thermoelectric performance. In particular, for 2% In_2S_3 doped Cu_2S (Cu_2S-2%In_2S_3), the power factor reaches as high as 1361 μW m^{-1} K^{-2} at 850 K, coupling with the moderate thermal conductivity of 0.95 W m^{-1} K^{-1} at 850 K, and the *ZT* value of 1.23 can be achieved at 850 K, which is more than 3.5 times higher than that of undoped Cu_2S at the same temperature. The high power factor of Cu_2S-2%In_2S_3 and decent *ZT*, along with suppression of phase transition and copper segregation, promises its practical applications in power generation.

Acknowledgements

We thank Professor Can Li for the access to Hall measurement instrument (HL5500PC), and thank Dr. Qike Jiang and Dr. Mingrun Li for the HR-TEM characterization. This work is financially supported by the National Natural Science Foundation of China (Grant No. 21273228 and 51290272) and 100 Talents Program of Chinese Academy of Sciences.

References

1. L. D. Zhao, G. J. Tan, S. Q. Hao, J. Q. He, Y. L. Pei, H. Chi, H.

Wang, S. K. Gong, H. B. Xu, V. P. Dravid, C. Uher, G. J. Snyder, C. Wolverton and M. G. Kanatzidis, *Science*, 2016, **351**, 141-144.
2. B. C. Sales, D. Mandrus and R. K. Williams, *Science*, 1996, **272**, 1325-1328.
3. G. S. Nolas, J. L. Cohn, G. A. Slack and S. B. Schujman, *Appl. Phys. Lett.*, 1998, **73**, 178-180.
4. D. M. Rowe and V. S. Shukla, *J. Appl. Phys.*, 1981, **52**, 7421-7426.
5. B. Poudel, Q. Hao, Y. Ma, Y. C. Lan, A. Minnich, B. Yu, X. A. Yan, D. Z. Wang, A. Muto, D. Vashaee, X. Y. Chen, J. M. Liu, M. S. Dresselhaus, G. Chen and Z. F. Ren, *Science*, 2008, **320**, 634-638.
6. L. D. Zhao, V. P. Dravid and M. G. Kanatzidis, *Energy Environ. Sci.*, 2014, **7**, 251-268.
7. J. Q. He, M. G. Kanatzidis and V. P. Dravid, *Mater. Today*, 2013, **16**, 166-176.
8. K. Biswas, J. Q. He, I. D. Blum, C.-I. Wu, T. P. Hogan, D. N. Seidman, V. P. Dravid and M. G. Kanatzidis, *Nature*, 2012, **490**, 414-418.
9. O. Delaire, J. Ma, K. Marty, A. F. May, M. A. McGuire, M. H. Du, D. J. Singh, A. Podlesnyak, G. Ehlers, M. D. Lumsden and B. C. Sales, *Nat. Mater.*, 2011, **10**, 614-619.
10. L. D. Zhao, S. H. Lo, Y. S. Zhang, H. Sun, G. J. Tan, C. Uher, C. Wolverton, V. P. Dravid and M. G. Kanatzidis, *Nature*, 2014, **508**, 373-377.
11. D. G. Cahill, P. V. Braun, G. Chen, D. R. Clarke, S. H. Fan, K. E. Goodson, P. Keblinski, W. P. King, G. D. Mahan, A. Majumdar, H. J. Maris, S. R. Phillpot, E. Pop and L. Shi, *Appl. Phys. Rev.*, 2014, **1**, 011305-011349.
12. A. I. Hochbaum, R. K. Chen, R. D. Delgado, W. J. Liang, E. C. Garnett, M. Najarian, A. Majumdar and P. D. Yang, *Nature*, 2008, **451**, 163-167.
13. D. L. Medlin and G. J. Snyder, *Curr. Opin. Colloid Interface Sci.*, 2009, **14**, 226-235.
14. J. P. Heremans, V. Jovovic, E. S. Toberer, A. Saramat, K. Kurosaki, A. Charoenphakdee, S. Yamanaka and G. J. Snyder, *Science*, 2008, **321**, 554-557.
15. C. J. Vineis, A. Shakouri, A. Majumdar and M. G. Kanatzidis, *Adv. Mater.*, 2010, **22**, 3970-3980.
16. D. Vashaee and A. Shakouri, *Phys. Rev. Lett.*, 2004, **92**, 106103-106106.
17. Y. Z. Pei, X. Y. Shi, A. LaLonde, H. Wang, L. D. Chen and G. J. Snyder, *Nature*, 2011, **473**, 66-69.
18. L. L. Zhao, X. L. Wang, F. Y. Fei, J. Y. Wang, Z. X. Cheng, S. X. Dou, J. Wang and G. J. Snyder, *J. Mater. Chem. A*, 2015, **3**, 9432-9437.
19. Y. He, T. Day, T. S. Zhang, H. L. Liu, X. Shi, L. D. Chen and G. J. Snyder, *Adv. Mater.*, 2014, **26**, 3974-3978.
20. Z. H. Ge, B. P. Zhang, Y. X. Chen, Z. X. Yu, Y. Liu and J. F. Li, *Chem. Commun.*, 2011, **47**, 12697-12699.
21. W. S. Liu, H. S. Kim, S. Chen, Q. Jie, B. Lv, M. L. Yao, Z. S. Ren, C. P. Opeil, S. Wilson, C. W. Chu and Z. F. Ren, *Proc. Natl. Acad. Sci. U. S. A.*, 2015, **112**, 3269-3274.
22. W. Liu, H. S. Kim, Q. Jie and Z. Ren, *Scr. Mater.*, 2016, **111**, 3-9.
23. G. Dennler, R. Chmielowski, S. Jacob, F. Capet, P. Roussel, S. Zastrow, K. Nielsch, I. Opahle and G. K. H. Madsen, *Adv. Energy. Mater.*, 2014, **4**, 1301581.
24. P. F. Qiu, X. Shi and L. D. Chen, *Energy Storage Materials*, 2016, **3**, 85-97.
25. G. J. Snyder and E. S. Toberer, *Nat. Mater.*, 2008, **7**, 105-114.
26. H. R. Yang, L. A. Jauregui, G. Q. Zhang, Y. P. Chen and Y. Wu, *Nano Lett.*, 2012, **12**, 540-545.
27. D. X. Liang, R. S. Ma, S. H. Jiao, G. S. Pang and S. H. Feng, *Nanoscale*, 2012, **4**, 6265-6268.
28. K. Suekuni, F. S. Kim, H. Nishiate, M. Ohta, H. I. Tanaka and T. Takabatake, *Appl. Phys. Lett.*, 2014, **105**, 132107.
29. Y. He, P. Lu, X. Shi, F. F. Xu, T. S. Zhang, G. J. Snyder, C. Uher and L. D. Chen, *Adv. Mater.*, 2015, **27**, 3639-3644.
30. H. S. Kim, Z. M. Gibbs, Y. L. Tang, H. Wang and G. J. Snyder, *Apl Mater.*, 2015, **3**, 041506.
31. P. F. Qiu, T. S. Zhang, Y. T. Qiu, X. Shi and L. D. Chen, *Energy Environ. Sci.*, 2014, **7**, 4000-4006.
32. M. Z. Bieniulis, C. E. Corry and E. R. Hoskins, *Geophys. Res. Lett.*, 1987, **14**, 135-138.
33. F. S. Liu, L. C. Pan, W. Q. Ao, L. P. He, X. X. Li, H. T. Li and J. Q. Li, *J. Electron. Mater.*, 2012, **41**, 2118-2125.
34. F. Liu, X. Y. Qin and D. Li, *J. Phys. D: Appl. Phys.*, 2007, **40**, 4974-4979.
35. J. Arbiol, J. Cerda, G. Dezanneau, A. Cirera, F. Peiro, A. Cornet and J. R. Morante, *J. Appl. Phys.*, 2002, **92**, 853-861.
36. R. RodriguezTalavera, S. Vargas, R. ArroyoMurillo, R. MontielCampos and E. HaroPoniatowski, *J. Mater. Res.*, 1997, **12**, 439-443.
37. M. K. Akhtar, S. E. Pratsinis and S. V. R. Mastrangelo, *J. Am. Ceram. Soc.*, 1992, **75**, 3408-3416.
38. S. Hishita, I. Mutoh, K. Koumoto and H. Yanagida, *Ceram. Int.*, 1983, **9**, 61-67.
39. Y. Iida and S. Ozaki, *J. Am. Ceram. Soc.*, 1961, **44**, 120-127.
40. A. W. Czanderna, C. N. R. Rao and J. M. Honig, *Trans. Faraday Soc.*, 1958, **54**, 1069-1073.
41. L. W. Wang, *Phys. Rev. Lett.*, 2012, **108**, 085703.
42. B. K. Chen, S. Chang, D. Y. Li, L. L. Chen, Y. T. Wang, T. Chen, B. S. Zou, H. Z. Zhong and A. L. Rogach, *Chem. Mater.*, 2015, **27**, 5949-5956.
43. A. D. P. Leach, L. G. Mast, E. A. Hernandez-Pagan and J. E. Macdonald, *J. Mater. Chem. C*, 2015, **3**, 3258-3265.

Graphitic Abstract

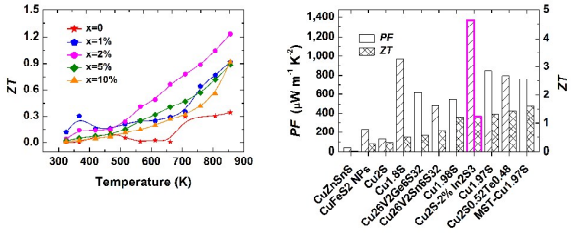

Simultaneously enhancing the power factor and thermoelectric performance of copper sulfide is realized by introducing In_2S_3, which will be beneficial to the practical application of Cu_2S.